



HAL
open science

Land-Atmosphere Cascade Fueled the 2020 Siberian Heatwave

L. Gloege, K. Kornhuber, O. Skulovich, I. Pal, S. Zhou, Philippe Ciais, P. Gentine

► **To cite this version:**

L. Gloege, K. Kornhuber, O. Skulovich, I. Pal, S. Zhou, et al.. Land-Atmosphere Cascade Fueled the 2020 Siberian Heatwave. AGU Advances, 2022, 3, 10.1029/2021AV000619 . insu-03993087

HAL Id: insu-03993087

<https://insu.hal.science/insu-03993087>

Submitted on 16 Feb 2023

HAL is a multi-disciplinary open access archive for the deposit and dissemination of scientific research documents, whether they are published or not. The documents may come from teaching and research institutions in France or abroad, or from public or private research centers.

L'archive ouverte pluridisciplinaire **HAL**, est destinée au dépôt et à la diffusion de documents scientifiques de niveau recherche, publiés ou non, émanant des établissements d'enseignement et de recherche français ou étrangers, des laboratoires publics ou privés.



Distributed under a Creative Commons Attribution - NoDerivatives 4.0 International License

Land-Atmosphere Cascade Fueled the 2020 Siberian Heatwave

L. Gloege^{1,2} , K. Kornhuber^{3,4} , O. Skulovich¹, I. Pal^{3,5} , S. Zhou¹ , P. Ciais⁶ , and P. Gentine¹ 

Key Points:

- Early warming favored early snowmelt, leading to earlier soil moisture availability and enhanced terrestrial greenness
- Soil moisture was depleted in late summer, leading to a drop in terrestrial greenness and increased browning
- The browning and reduced soil moisture in summer reduced evapotranspiration and increased sensible heat flux, further fueling the heatwave

Supporting Information:

Supporting Information may be found in the online version of this article.

Correspondence to:

L. Gloege,
ljg2157@columbia.edu

Citation:

Gloege, L., Kornhuber, K., Skulovich, O., Pal, I., Zhou, S., Ciais, P., & Gentine, P. (2022). Land-atmosphere cascade fueled the 2020 Siberian heatwave. *AGU Advances*, 3, e2021AV000619. <https://doi.org/10.1029/2021AV000619>

Received 29 NOV 2021
Accepted 23 SEP 2022

Peer Review The peer review history for this article is available as a PDF in the Supporting Information.

Author Contributions:

Conceptualization: L. Gloege, K. Kornhuber, O. Skulovich, I. Pal, S. Zhou, P. Ciais, P. Gentine
Data curation: L. Gloege
Formal analysis: L. Gloege, K. Kornhuber, O. Skulovich, S. Zhou, P. Gentine
Funding acquisition: P. Gentine

© 2022. The Authors.

This is an open access article under the terms of the [Creative Commons Attribution-NonCommercial License](https://creativecommons.org/licenses/by-nc/4.0/), which permits use, distribution and reproduction in any medium, provided the original work is properly cited and is not used for commercial purposes.

¹Columbia University, New York, NY, USA, ²Open Earth Foundation, Marina del Rey, CA, USA, ³The Earth Institute, Columbia University, New York, NY, USA, ⁴German Council on Foreign Relations, Berlin, Germany, ⁵NOAA Center for Earth System Sciences and Remote Sensing Technologies, The City University of New York CREST Institute, New York, NY, USA, ⁶Laboratoire des Sciences du Climat et de l'Environnement, Saclay, France

Abstract A heatwave in Siberia starting in January 2020, initiated by a wave 5 pattern in the jet stream, caused the surface air temperature to reach 38°C in June with important impacts on ecosystems and water resources. Here we show that this dynamical setup started a chain of events leading to this long-lasting and unusual event: positive temperature anomalies over Siberia caused early snowmelt, leading to substantial earlier vegetation greening accompanied by decreased soil moisture and browning in the summer. This soil moisture depletion and vegetation browning, in turn, increased the impact of the heatwave on the atmosphere through a land-atmosphere feedback. This line of evidence suggests that large-scale dynamics and land-atmosphere interactions both contributed to the magnitude and persistence of this record-breaking heatwave, in addition to the background global warming impact on mean temperature. Here, we describe a carry-over effect in Siberia from a spring positive temperature anomaly into summer dryness and browning, with retroaction into the atmosphere. With the Arctic warming twice as fast as the global average, this event foreshadows the future of northern latitude continents and emphasizes the importance of both atmospheric dynamics and land-atmosphere interactions in the future as the climate changes. More frequent similar events could have major consequences on the carbon cycle in these carbon-rich northern latitude regions.

Plain Language Summary A heatwave starting January 2020 in Siberia caused temperatures to reach 38°C (100°F) in June. The winter heatwave caused an early snow melt which elevated the soil moisture. This in turn caused earlier spring greening. As the heatwave persisted, soil moisture evaporated causing soil to be drier and trees to brown earlier in summer. Since the soil was drier than normal, the heat emanating from it was elevated which further exacerbated the heatwave. With arctic temperatures increasing twice as fast as the global average, the role of land-atmosphere interactions we describe will likely become more prominent in the future as the climate warms.

1. Introduction

The frequency and intensity of heatwaves has increased in recent decades; due to climate change increasing not only the global mean temperature but also its variability (Baldwin et al., 2019; Ciavarella et al., 2020; Easterling et al., 2000; Rahmstorf & Coumou, 2011; Schär et al., 2004; Stott et al., 2004; Van Oldenborgh et al., 2019). Additional warming is expected to increase the duration and intensity of heatwaves in the coming decades (Horton et al., 2016; Perkins-Kirkpatrick & Gibson, 2017). This has the potential to strain the terrestrial biosphere (Zscheischler et al., 2014) and limit its capacity to mitigate future climate change through carbon sequestration (Friedlingstein et al., 2019), via reduced photosynthesis, increased ecosystem respiration, and an increase in wildfires.

In 2020, a mega-heatwave, here defined as an intense and persistent heatwave (Miralles et al., 2014), caused the surface air temperature (SAT) to reach a record-breaking 38°C in Verkhoysk Siberia on 20 June 2020 (Ciavarella et al., 2020). This mega-heatwave was initiated by a strong stratospheric polar vortex and tropospheric jet stream from January through April (Overland & Wang, 2021). Integral to mid-latitude heatwave development is an atmospheric blocking event, where a high-pressure system remains near-stationary for days or even weeks (Black et al., 2004). The 2020 Siberian heatwave was later associated with a blocking event in June and a northward swing in the jet stream sending warm air into the region (Ciavarella et al., 2020).

Here, we show that the early heatwave in Siberia, induced by a persistent meridional wind ridge, led to a carry-over effect on the June heatwave through a series of land-atmosphere feedbacks. The early heatwave generated a

Methodology: L. Gloege, K. Kornhuber, O. Skulovich, I. Pal, S. Zhou, P. Ciais, P. Gentine

Supervision: P. Gentine

Visualization: L. Gloege, K. Kornhuber, O. Skulovich, S. Zhou

Writing – original draft: L. Gloege

Writing – review & editing: L. Gloege, K. Kornhuber, O. Skulovich, I. Pal, S. Zhou, P. Ciais, P. Gentine

cascade of events that further amplified the late spring heatwave. The initial and persistent heat anomaly caused earlier snowmelt, leading to an earlier increase in soil moisture and vegetation activity. This increased vegetation activity, led to a draw-down in soil moisture that Granger-caused (Section 2) a decrease in terrestrial greenness three months later. This led to substantial vegetation browning and drier soil conditions, unusual at those high northern latitudes; generating reduced surface evapotranspiration and increased sensible heat flux. This fed back onto the atmosphere and amplified the late spring heatwave through land-atmosphere feedbacks.

2. Methods

2.1. Datasets

The ERA5 reanalysis (Hersbach et al., 2020), produced by the European Centre for Medium-Range Weather Forecasts (ECMWF), combines observations from across the globe with model output into a globally complete and consistent data set. Output is provided hourly on a 0.25° grid. We extracted 2-m air temperature, soil moisture, snowmelt, 10-m (longitudinal) u-component, and 10-m (latitudinal) v-component of wind. Each product was re-gridded to a daily temporal resolution with a 1° spatial resolution.

Leaf area index (LAI) is an essential climate variable (Belward et al., 2016) which measures amount of foliage as a measure for the photosynthetic active area. LAI is based on the National Oceanic and Atmospheric Administration Climate Data Record (NOAA-CDR) data set version 5 (Vermote, 2019) and estimated using surface reflectance data from Advanced Very-High-Resolution Radiometer (AVHRR) data aboard eight NOAA polar-orbiting satellites (NOAA-7, -9, -11, -14, -16, -17, -18, and -19) using an artificial neural network. The algorithm has been validated using both in situ data and the Moderate Resolution Imaging Spectroradiometer LAI (Claverie et al., 2016). The AVHRR-based data set is provided from 1982 to the present at 0.05° (5 km) resolution; we regrid the product to daily resolution at 1° spatial resolution. Only years 2001-present were analyzed to avoid biases and drift from satellites not equipped with a propulsion system to maintain orbit.

2.2. Dry Static Energy Convergence

Atmospheric horizontal heat transport was diagnosed as dry static energy convergence (EC), calculated as the negative divergence of vertically integrated dry static energy flux over the pressure (p) from the top of the atmosphere ($p = 0$) to the surface ($p = p_s$):

$$EC = -\nabla \cdot \int_0^{p_s} (\mathbf{u}s) dp$$

$$s = c_p \cdot T + g_0 \cdot z$$

where $\nabla \cdot$ is the horizontal divergence operator, \mathbf{u} is the horizontal vector wind, s is dry static energy, c_p is specific heat capacity of dry air, T is air temperature, g_0 is gravitational acceleration constant, and z is geopotential height.

Using monthly \mathbf{u} and s and their climatological monthly values over 1981–2010 as reference, we calculated monthly EC anomalies (ΔEC) in 2020 and further decomposed them into three components: (a) a thermodynamic term (ΔTH) induced by dry static energy anomalies, (b) a dynamic term (ΔMCD) induced by horizontal wind anomalies, and (c) a cross term (ΔCRO) induced by the product of specific humidity anomalies and horizontal wind anomalies:

$$\Delta EC \approx -\nabla \cdot \int_0^{p_s} (\mathbf{u}_0 \Delta s + s_0 \Delta \mathbf{u} + \Delta \mathbf{u} \Delta s) dp$$

$$\Delta TH = -\nabla \cdot \int_0^{p_s} (\mathbf{u}_0 \Delta s) dp$$

$$\Delta MCD = -\nabla \cdot \int_0^{p_s} (s_0 \Delta \mathbf{u}) dp$$

$$\Delta CRO = -\nabla \cdot \int_0^{p_s} (\Delta \mathbf{u} \Delta s) dp$$

where the subscript 0 represents climatological monthly values and Δ represents departure from the monthly climatology.

2.3. Granger Causality

Granger causality tests the usefulness of a variable to forecast another. If the variable is useful, then we say it Granger-causes another. Causal here is in the statistical sense and does not necessarily mean there is a physical causal relationship. It is also important to keep in mind this statistical test cannot account for confounding variables.

We use Granger causality to quantify the causal impact of soil moisture on LAI. Given variables X and Y with two time series, Granger causality tests whether past values of X affects the current value of Y . If so, we say that X Granger-causes Y . This is accomplished by comparing two models, an unrestricted and restricted model. The unrestricted model assumes the current value of Y at time t is influenced by previous values of X and Y :

$$Y_t = \alpha + \delta t + \phi_1 Y_{t-1} + \dots + \phi_p Y_{t-p} + \beta_1 X_{t-1} + \dots + \beta_q X_{t-q} + \epsilon_t$$

and a restricted model where the current value of Y is only influenced by previous values of Y , as well as an intercept (α) and time (δt):

$$Y_t = \alpha + \delta t + \phi_1 Y_{t-1} + \dots + \phi_p Y_{t-p} + \epsilon_t$$

Sum of squared residuals (SSR), Akaike information criterion (AIC), and Bayesian information criterion (BIC) are used for model selection to estimate the relative quality of the unrestricted and restricted models. BIC is similar to AIC, however it adds a higher penalty for models with more parameters. If SSR, AIC, and BIC are lower for the unrestricted model, then we can conclude that X Granger-causes Y . This analysis was facilitated by the Python statsmodels package (Seabold & Perktold, 2010) and performed by averaging the LAI and soil moisture within a large region (50°N–75°N, 50°E–120°E).

3. Spring Drivers and Larger-Scale Patterns

Surface air temperature (SAT) conditions in Eurasia were anomalously high from January–June 2020 (Overland & Wang, 2021). The SAT anomaly over the period from 25 May 2020 through 7 June 2020 exceeded +6°C in Siberia (Figures 1a and 1b). A persistent and strong stratospheric polar vortex contributed to above normal SAT in Eurasia throughout winter and spring 2020 (Ciavarella et al., 2020; Overland & Wang, 2021), keeping the cold air over the Arctic. From April 2020 to May 2020 a strong meandering jet, characterized by an amplified Rossby wave 5 (Kornhuber & Tamarin-Brodsky, 2020) developed and remained stationary over large parts of the Northern Hemisphere (NH) (Figure 1c). The increase in wave 5 amplitude (Figure 1c) co-occurred with the record breaking temperatures in early spring, and throughout the summer (Figure 1d). Wave 5 has a preferred phase position and is thereby associated with record temperatures over Russia. This near circum-global pattern connected below average cold temperatures on the North American East coast and record warm anomalies over central Eurasia. The latter kick-started a series of heat records within the Arctic circle (Ciavarella et al., 2020). Also, the Arctic Oscillation was in a strong positive phase, which is known to favor Eurasian summer heatwaves (Wu & Chen, 2020).

We attribute atmospheric dynamics to the large horizontal heat transport into Siberia in early spring (Figure 2a), suggesting that a ridging pattern largely defined the onset and initial persistence of the heatwave. A persistent high pressure system was parked over the area, which elevated SAT anomalies in Siberia.

4. Impact of Heatwave on Snowmelt and Soil Moisture

In March–May 2020, the high positive SAT anomalies (Figure 1b) induced early snowmelt relative to climatology (Figure 3a) and reduced snow cover (Figure 3b) within the study region extending from 50°N–75°N and 50°E–120°E. This sharp drop in snow aligned with the heatwave period over Siberia (Overland & Wang, 2021). In the Northern Hemisphere, snow mass has been decreasing since 1980 while regionally it has been increasing in east Siberia (Pulliainen et al., 2020). Snow cover anomalies relative to climatology were reduced in the southeast

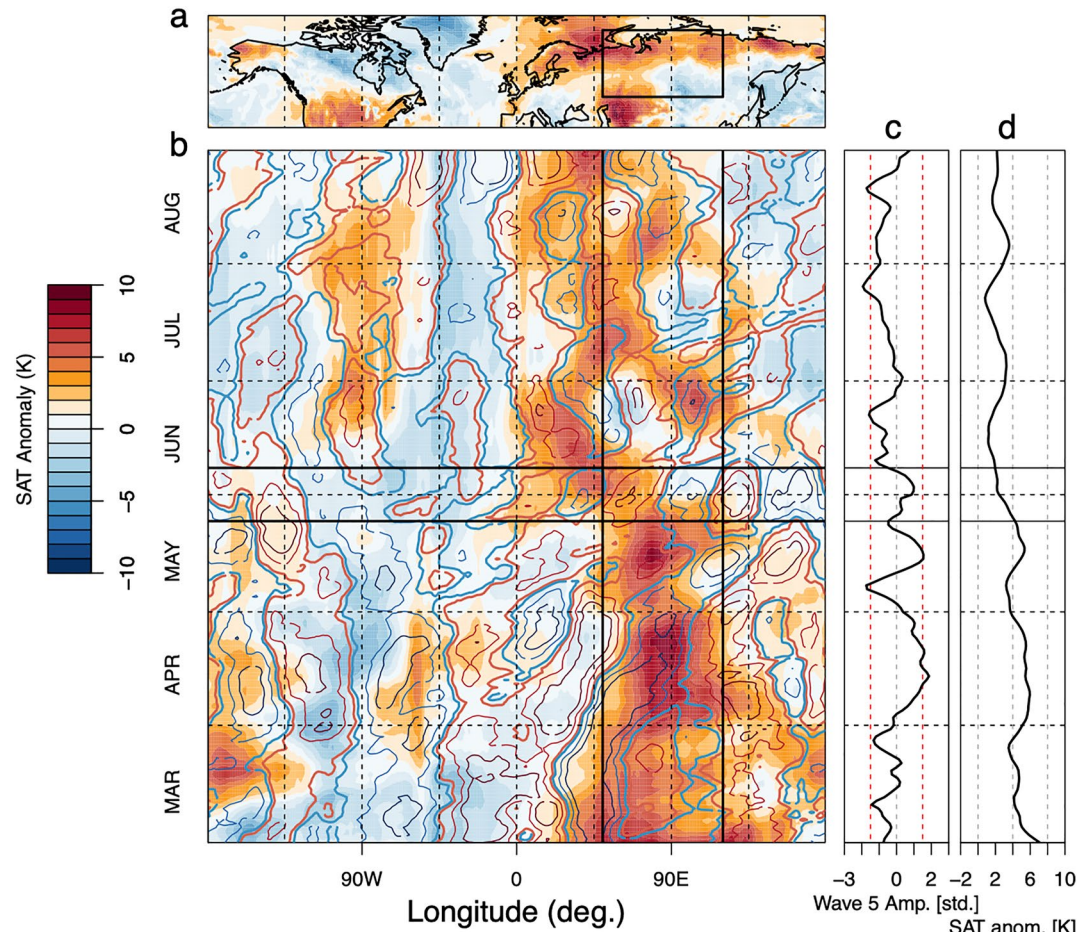


Figure 1. Northern Hemisphere surface air temperature and large scale atmospheric circulation in spring to summer 2020: (a) 7-day mean 2 m surface air temperature anomaly centered on May 31st. (b) Hovmoeller diagram of 7 days running mean values of SAT averaged over 40°N–70°N overlaid with contours of meridional wind speed averaged over 37.5°N–57.5°N. Contours denote the –11, –6, –1 m/s (blue) and 1, 6, 11 m/s (red) levels respectively. Solid black horizontal lines denote the time period shown in (a), solid black vertical lines show the 50°–120°E area as shown in (a) for orientation. (c) Amplitude of Rossby Wave number 5 in units of standard deviation (std.) relative to monthly climatology. Red dashed lines denote 1.5 standard deviation departures from the mean for orientation. (d) SAT anomaly averaged over 50°E–120°E, 40°–70°N (also see black box in a)). In April to May a persistent wave train diagnosed as a high wave 5 amplitudes corresponds to a rise in temperatures over central Eurasia.

corner of the study region (50°E–120°E, 50°N–75°N) starting in March (Figure S1a in Supporting Information S1) and progressing toward the northeast from April through June (Figures S1b, S1c, and S1d in Supporting Information S1). The regional warming resulted in an evolving pattern of soil moisture across the same region: Eastern Europe experienced low soil moisture anomalies in March and April (Figures 3c and 3d) and elevated soil moisture in May and June due to early snowmelt (Figures 3e and 3f), while southwest Siberia showed anomalously low soil moisture and southeast Siberia had elevated soil moisture (Figures 3c–3f), due to earlier snowmelt.

To further explore the response of the various soil moisture patterns to the heatwave and snowmelt, time series of soil moisture and snowmelt from the ERA5 reanalysis over three contrasting regions are investigated within the period 1981–2020: Northwestern Russia, Western Siberia, and Northeastern Siberia (see Figure 3c for locations). In Northwestern Russia, the wetness in late spring and early summer (Figure 3g) was a result of earlier snowmelt (Figure 3a) that led to soil moisture depletion in June 2020 but later to a recovery to the climatological mean. This region represents a restoration pattern with the effects of the spring heatwave dissipating with time. The soil moisture in western Siberia peaked in March 2020 and remained drier than normal from April to October of that year (Figure 3h). In that region, May 2020 also experienced the least snow cover (Figure S1c in Supporting Information S1) leading up to persistent summer dryness (Figure 3h) and gradual restoration to climatology in fall. In

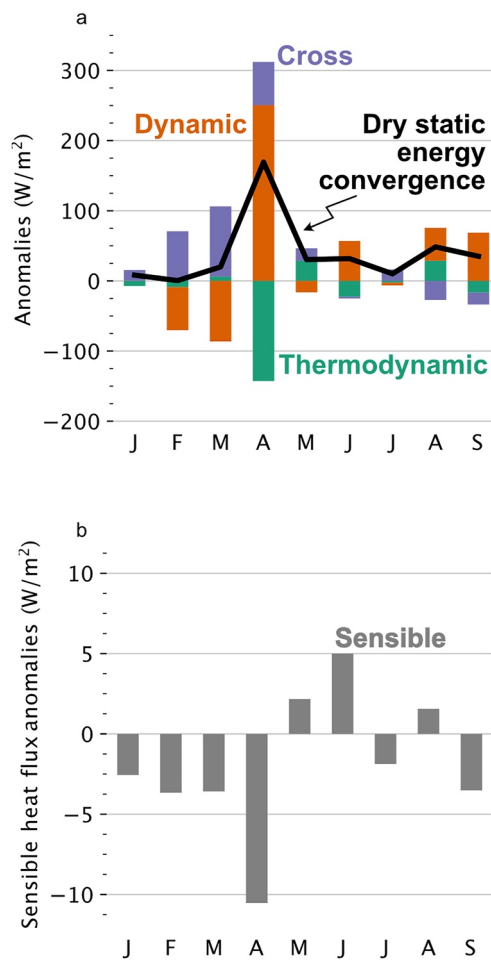


Figure 2. (a) Monthly anomalies of dry static energy convergence in 2020 and its components averaged within 50–75°N, 50–120°E. (b) Sensible heat flux anomalies. Sensible heat flux anomaly was negative (downward) January–April, which contributed early snowmelt. A positive (upward) sensible heat flux anomaly in May and June enhanced the intensity of the heatwave.

Northeastern Siberia, soil moisture was elevated in May 2020 (Figure 3i) as the snowmelt peaked almost a month earlier compared to its climatology in response to the heatwave (Figure 3a). Over the 2001–2020 record, 2020 was the fifth driest June on record (Figure S4 in Supporting Information S1) and the driest fall with the soil moisture remaining below mean values. The earlier peak soil moisture increase over the region was induced by the earlier timing of snowmelt. After peaking, soil moisture rapidly depleted (Figures 3c–3f) through losses to vegetation transpiration and evaporation. Soil moisture was elevated in March and April of 2020 with Negative anomalies beginning in May 2020. To summarize this section, wetness was observed in spring from an early snowmelt and then changed to dryness in summer. The next section explores the role of soil moisture in causing vegetation greening in spring and browning in late summer.

5. Impact on Terrestrial Greenness

Simultaneously, the early snowmelt that elevated soil moisture created favorable conditions for photosynthetic activity and greening. Many studies show early snowmelt causes spring greening (Pulliainen et al., 2017; Barichivich et al., 2014; Grippa et al., 2005; X. Zhang et al., 2019). Vegetation activity was substantially and positively impacted by the heatwave in spring and summer due to the evolving pattern of soil moisture. We use LAI, the ratio of leaf area per unit ground area, and an important indicator of vegetation health status (Section 2), as a proxy for terrestrial greenness.

In May and June of 2020, LAI was higher than normal within the study region, bounded between 50°N and 75°N and 50°E–120°E (Figure 4a). The enhanced LAI was localized to Siberia, with lower values found in Europe (Figure 4b). In May of 2020, the study region saw a widespread increase in LAI relative to climatology (Figure 4b). The timing of the greening closely follows the increase in snowmelt in the previous month (Figure S2 in Supporting Information S1) and concomitant availability of soil moisture and earlier availability of favorable temperatures for photosynthesis (Figure 1).

As a result, in 2020, the seasonal cycle of LAI was shifted. LAI achieved a maximum value of 3.4 in May at (58°N, 90°E) (Figure S3 in Supporting Information S1). This is 130% greater than the May climatological value of 1.4 at this location. In August 2020 at this location LAI was 2.7, which is 26% lower than its climatology. In August, at (55°N, 95°E) LAI reached a minimum value of 1.08, which is 71% less than the climatological value (3.8) at this time. This lower than normal LAI is largely found in the Taiga forest of Eastern Siberia. These changes also hold within the region 50°N–75°N and 50°E–120°E, where LAI was anomalously low in August 2020 (Figure 4a). The percent change in LAI relative to climatology begins to decrease in June and July of 2020 (Figures 4c and 4d). However, high northern latitude regions experienced elevated LAI in June. In August, LAI is anomalously low (Figure 4e), corresponding to the region of dry soil moisture (Figure 3e) in the summer due to the earlier snowmelt.

We further test the causal link between time series of soil moisture and LAI with Granger causality (Section 2) to investigate whether positive soil moisture anomalies in the spring, due to a temperature anomaly, caused this earlier greening and later browning. Based on this analysis (Section 2), we conclude that soil moisture Granger-caused the LAI anomaly with a lead time of three months over the studied region (50°E–120°E, 50°N–75°N) (Figure S5 in Supporting Information S1), similar to the lag between snowmelt and soil moisture due to the initial SAT anomaly. This emphasizes the role of initial soil moisture anomalies on LAI, itself triggered by the chain of events starting with the initial heatwave anomaly in late winter and early spring. Atmospheric aridity may also play an additional role in explaining the reduction in LAI (Zhou, Williams, et al., 2019; Zhou, Zhang, et al., 2019).

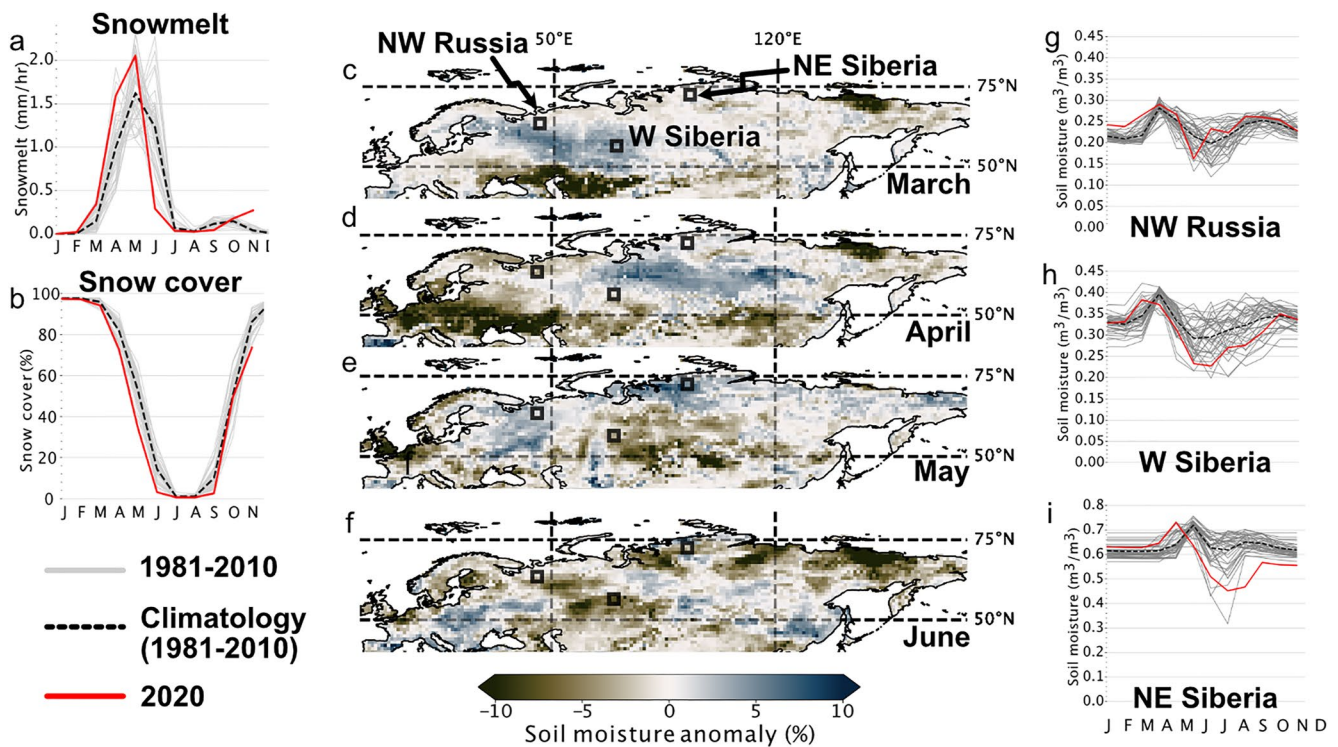


Figure 3. Monthly average (a) Snowmelt and (b) snow cover for years 1981–2020 using data within the study region (50°N–75°N and 50°E–120°E). Gray lines indicate the years 1981–2019, with the dashed line indicating the 1981–2010 climatology. Red line indicates 2020. Soil moisture anomalies from 1981 to 2010 mean are shown for (c–f) March through June. Dashed line delineates the study region. Small black boxes show the location of three regions, whose time series are shown in (g–i). Elevated soil moisture is observed in March and April transitioning to dryness in May and June.

The earlier greening increased evapotranspiration which led to a depletion in soil moisture (Figure 3f) which then led to plant stress and reduced LAI in the summer (Figures 4a and 4e). When averaged over the region, 50°N–75°N and 50°E–120°E, June 2020 is in the 23rd percentile across all Junes from 2001 to 2020 (Figure S4 in Supporting Information S1). In addition, the surface sensible heat flux anomaly became positive and peaked in June (Figure 2), coinciding with the peak of the heatwave. This led to an important contribution attributable to the surface sensible heat flux and therefore from land-atmosphere interactions to the summer heatwave in the region (Figure 2). Sensible heat represents the primary means of heat transfer between the surface and the overlying air to the thermal gradient. This soil moisture-vegetation-temperature feedback amplified air temperature via reduced evaporative cooling and increased sensible heat flux (Figure 5) (Fischer et al., 2007; Stéfanon et al., 2014). August 2020 was the warmest August in the last 20 years, while August LAI was the lowest over the same period (Figure S4 in Supporting Information S1). In mid-latitude regions, soil moisture drought is known to have strong influence on the intensity of temperature extremes (Lorenz et al., 2016), which can be advected to cooler regions downwind and enhance the heatwave (Schumacher et al., 2019). Thus, even in Siberia, the 2020 summer reduction in soil moisture (Figure 3) and increase in vegetation browning (Figure 4) amplified the heatwave, further stressing vegetation.

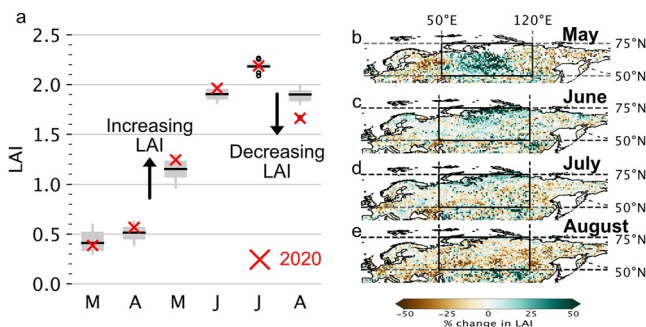


Figure 4. (a) Box plots of AVHRR-based LAI estimates from 2001 to 2019 using data within 50°N–75°N and 50°E–120°E. Observations prior to 2001 were excluded (see Section 2). Black line is the median across these years. Small circles indicate outliers, which are greater than 1.5 times the interquartile range. Red x's indicate LAI in 2020. Percent change in LAI from 2001 to 2019 climatology for May, June, July, and August 2020 (b–e). Black boxes indicate analysis region (50°N–75°N and 50°E–120°E) considered in this study. Enhanced greening is observed in May while enhanced browning is observed in August.

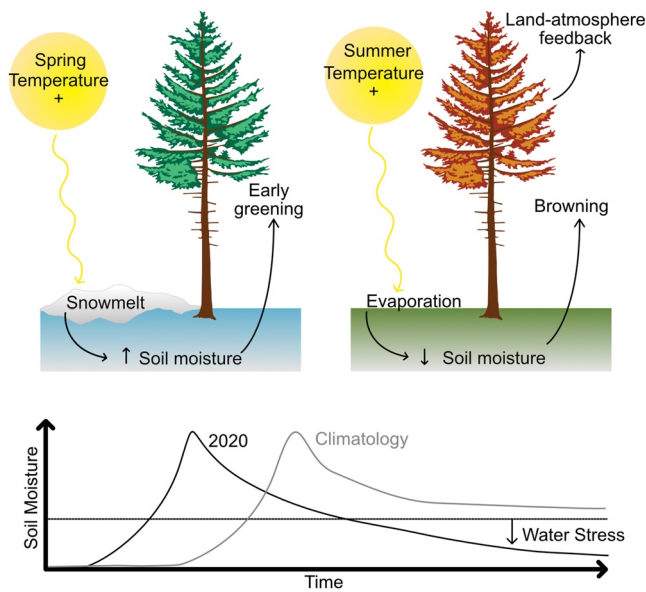


Figure 5. Schematic illustrating increased spring temperature leads to an early snow melt, which increases soil moisture causing an early greening. In summer, the enhanced temperature draws down soil moisture through evaporation which leads to browning and a land-atmosphere feedback. Early snow melt and a persistent heatwave causes water stress in summer relative to climatology.

Supporting Information S1). These soil moisture anomalies Granger-caused changes in the LAI, which was anomalously high in spring and low in summer (Figure S4a in Supporting Information S1). Compared to August of every other year, 2020 had the lowest August LAI (Figure S4f in Supporting Information S1). The low summer LAI, and hence browning, reduced evapotranspiration causing an anomalously highly sensible heat flux in June, which further amplified the heatwave, as emphasized by an attribution analysis (Section 2) (Figure 2). The chain of events starting in the spring and extending to the summer is summarized and illustrated in Figure 5.

6. Implications

In the future, the areal extent of blocking events is projected to increase by as much as 17%, thereby increasing the areal extent of heatwaves (Nabizadeh et al., 2019). Northern latitude regions have witnessed a much more rapid increase in air temperature compared to the rest of the globe, referred to as the Arctic amplification (Serreze & Barry, 2011). The combination of Arctic amplification, and increased frequency and intensity of extremes could potentially place substantial pressure on northern latitudes ecosystems, such as boreal forests. The combined stress could potentially lead to an ecosystem tipping point (Lenton et al., 2008), reverting northern latitude CO₂ uptake capacity (P. Zhang, Jeong, et al., 2020) into a source to the atmosphere, especially if the permafrost were to melt (Keuper et al., 2020; Turetsky et al., 2020). North of Siberia's tree line, the 2020 fire season began early due to warming temperatures which re-emerged “zombie fires” in the peatland (McCarty et al., 2020; Witze, 2020), which smolder through the

non-fire season and intensify in the subsequent spring. This carbon-rich peatland region is currently a net sink for atmospheric CO₂; yet this region could become a net source by the end of the century (Hugelius et al., 2020) as the climate warms and if wildfire frequency were to increase (Sherstyukov & Sherstyukov, 2014) and be as dramatic as in 2020. Sustained heatwaves with magnitudes comparable to 2020 could in turn impact northern latitude surface processes such as snow cover, terrestrial greenness, or wildfire frequency and intensity (Lange et al., 2020).

Soil moisture, soil temperature, land use, land cover, nutrient availability, and vegetation are drivers of soil emissions (Oertel et al., 2016). Heatwave induced soil heating has the potential to increase emissions through enhanced connection with deep-soil carbon stocks being activated by deeper aeration (Castellano et al., 2019). However, this influence could be counter-balanced by soil moisture availability. Green et al. (2019) show that the level of soil moisture has a large negative influence on the land's ability to store carbon. Drier soils will reduce methane and CO₂ emissions (Oh et al., 2020; Selsted et al., 2012; Zona et al., 2016). In the Arctic, significant declines in net ecosystem productivity beginning in 2013 are driven by increased heterotrophic respiration arising from increased precipitation and warming (Larson et al., 2021). In tundra environments and landscapes recently affected by fire, soil respiration often exceeded gross primary production (GPP), resulting in a net annual source of CO₂ to the atmosphere. As this region continues to warm, soil respiration may increasingly offset GPP, further amplifying global climate change (Watts et al., 2021).

Given current policies, we are likely on track with Representative Concentration Pathway 4.5 or 6.0 (RCP4.5–6.0) (Hausfather & Peters, 2020), with an increase in global temperature of about 3°C by the end of the century. More frequent and severe heatwaves are to be expected as global temperatures increase throughout the 21st century (Collins et al., 2013) but also as climate variability increases (Schär et al., 2004). To assess the impact of future heatwaves in sparsely sampled regions, such as Siberia, we must rely on process-based models, that is, Earth system models. However, correctly representing atmospheric processes and land-atmosphere feedbacks remains challenging in Earth system models (Davini & D'Andrea, 2016, 2020). Current generation models have difficulties capturing extreme events due to atmospheric dynamic anomalies (Mann et al., 2018; Schewe et al., 2019), correctly capturing blocking events (Davini & D'Andrea, 2016, 2020; Hanna et al., 2018), as well as vegetation feedbacks, and snow/precipitation dynamics. Mean heatwave frequency is also underestimated in Earth

system models, with region-dependent biases for mean heatwave duration, intensity, and cumulative heat (Hirsch et al., 2021). In addition, even ERA5 does not include several important processes, such as dynamic phenology, but instead uses prescribed monthly climatology (Boussetta et al., 2013). An increase in observational constraints and improved parameterizations will lead to more accurate models, which are critical to assess the impact of extremes in real-time and also their future projections.

7. Conclusions

To summarize, we show that an early warming anomaly in Siberia and northern Eurasia due to a phase-locked wave 5 pattern in the jet stream (Kornhuber & Tamarin-Brodsky, 2020) favored earlier snowmelt, which led to increased spring soil moisture and increased terrestrial greenness. In the later part of the summer, soil moisture was depleted leading to a drop in terrestrial greenness and increased vegetation browning. This water stress decreased LAI, since dryness stress from low soil moisture limits vegetation growth and can lead to vegetation browning and senescence (Liu et al., 2020), as schematized in Figure 5. This heatwave induced a drop in terrestrial activity, which may not necessarily hold in all regions, as the response of different ecosystems to drought is dependent on the species composition and resistance to water stress (Bastos et al., 2020; Konings et al., 2017), as well as on the ratio between water supply from precipitation and water demand from the atmosphere (Y. Zhang, Parazoo, et al., 2020).

This manuscript presents a documentation of carry-over effects from spring temperature anomalies leading to summer dryness and browning in Siberia, which further contributed to fueling elevated summer temperatures (Figure S4 in Supporting Information S1). Early snowmelt leading to spring greening is well established (Barichivich et al., 2014; Grippa et al., 2005; Pulliainen et al., 2017), while spring soil-moisture exhaustion leading to dryness has been documented in Europe (Bastos et al., 2020). Anomalously low soil moisture has occurred before 2020, yet greening exhausting soil moisture and then browning in summer in Siberia has not been previously documented in the literature. This feedback and cascading effect in Siberia is unique to 2020, especially considering the region is conventionally considered cold and wet. Legacy effects could further impact such events, which we leave for future research.

Conflict of Interest

The authors declare no conflicts of interest relevant to this study.

Data Availability Statement

ERA5-land reanalysis fields with hourly temporal resolution can be downloaded from the Copernicus Climate Change Service (C3S) Climate Data Store (<https://cds.climate.copernicus.eu/%23%21/search%3Ftext%3DERA5%26type%3Ddataset>). Leaf area index (LAI) climate date record (CDR) can be downloaded from NOAA National Center for Environmental Information (NCEI) (<https://www.ncei.noaa.gov/products/climate-data-records/leaf-area-index-and-fapar>).

References

- Baldwin, J. W., Dessy, J. B., Vecchi, G. A., & Oppenheimer, M. (2019). Temporally compound heat wave events and global warming: An emerging hazard. *Earth's Future*, 7(4), 411–427. <https://doi.org/10.1029/2018ef000989>
- Barichivich, J., Briffa, K. R., Myneni, R., Schrier, G. V. d., Dorigo, W., Tucker, C. J., et al. (2014). Temperature and snow-mediated moisture controls of summer photosynthetic activity in northern terrestrial ecosystems between 1982 and 2011. *Remote Sensing*, 6(2), 1390–1431. <https://doi.org/10.3390/rs6021390>
- Bastos, A., Ciais, P., Friedlingstein, P., Sitch, S., Pongratz, J., Fan, L., et al. (2020). Direct and seasonal legacy effects of the 2018 heat wave and drought on European ecosystem productivity. *Science Advances*, 6(24), eaba2724. <https://doi.org/10.1126/sciadv.aba2724>
- Belward, A., Bourassa, M. A., Dowell, M., Briggs, S., Dolman, H., Holmlund, K., et al. (2016). The global observing system for climate: Implementation needs. *GCOS-200*, 342.
- Black, E., Blackburn, M., Harrison, G., Hoskins, B., & Methven, J. (2004). Factors contributing to the summer 2003 European heatwave. *Weather*, 59(8), 217–223. <https://doi.org/10.1256/wea.74.04>
- Boussetta, S., Balsamo, G., Beljaars, A., Kral, T., & Jarlan, L. (2013). Impact of a satellite-derived leaf area index monthly climatology in a global numerical weather prediction model. *International Journal of Remote Sensing*, 34(9–10), 3520–3542. <https://doi.org/10.1080/01431161.2012.716543>
- Castellano, M. J., Archontoulis, S. V., Helmers, M. J., Poffenbarger, H. J., & Six, J. (2019). Sustainable intensification of agricultural drainage. *Nature Sustainability*, 2(10), 914–921. <https://doi.org/10.1038/s41893-019-0393-0>

Acknowledgments

Funding for this study was provided by the European Research Council (ERC) Synergy Grant “Understanding and Modelling the Earth System with Machine Learning (USMILE)” under the Horizon 2020 research and innovation programme (Grant agreement No. 855187). K.K was partially supported by NSF project NSF AGS-1934358.

- Ciavarella, A., Cotterill, D., Stott, P., Kew, S., Philip, S., van Oldenborgh, G. J., et al. (2020). *Siberian heatwave of 2020 almost impossible without climate change*. World Weather Attribution Organization. Retrieved from <https://www.worldweatherattribution.org/siberian-heatwave-of-2020-almost-impossible-without-climate-change>
- Claverie, M., Matthews, J. L., Vermote, E. F., & Justice, C. O. (2016). A 30+ year AVHRR LAI and FAPAR climate data record: Algorithm description and validation. *Remote Sensing*, 8(3), 263. <https://doi.org/10.3390/rs8030263>
- Collins, M., Knutti, R., Arblaster, J., Dufresne, J.-L., Fichet, T., Friedlingstein, P., et al. (2013). Long-term climate change: Projections, commitments and irreversibility. In *Climate change 2013-the physical science basis: Contribution of working group i to the fifth assessment report of the intergovernmental panel on climate change* (pp. 1029–1136). Cambridge University Press.
- Davini, P., & D'Andrea, F. (2016). Northern Hemisphere atmospheric blocking representation in global climate models: Twenty years of improvements? *Journal of Climate*, 29(24), 8823–8840. <https://doi.org/10.1175/jcli-d-16-0242.1>
- Davini, P., & D'Andrea, F. (2020). From CMIP3 to CMIP6: Northern Hemisphere atmospheric blocking simulation in present and future climate. *Journal of Climate*, 33(23), 10021–10038. <https://doi.org/10.1175/jcli-d-19-0862.1>
- Easterling, D. R., Evans, J. L., Groisman, P. Y., Karl, T. R., Kunkel, K. E., & Ambenje, P. (2000). Observed variability and trends in extreme climate events: A brief review. *Bulletin of the American Meteorological Society*, 81(3), 417–426. [https://doi.org/10.1175/1520-0477\(2000\)081<0417:ovatie>2.3.co;2](https://doi.org/10.1175/1520-0477(2000)081<0417:ovatie>2.3.co;2)
- Fischer, E. M., Seneviratne, S. I., Lüthi, D., & Schär, C. (2007). Contribution of land-atmosphere coupling to recent European summer heat waves. *Geophysical Research Letters*, 34(6), L06707. <https://doi.org/10.1029/2006gl029068>
- Friedlingstein, P., Jones, M., O'sullivan, M., Andrew, R., Hauck, J., Peters, G., et al. (2019). Global carbon budget 2019. *Earth System Science Data*, 11(4), 1783–1838. <https://doi.org/10.5194/essd-11-1783-2019>
- Green, J. K., Seneviratne, S. I., Berg, A. M., Findell, K. L., Hagemann, S., Lawrence, D. M., & Gentine, P. (2019). Large influence of soil moisture on long-term terrestrial carbon uptake. *Nature*, 565(7740), 476–479. <https://doi.org/10.1038/s41586-018-0848-x>
- Grippa, M., Kergoat, L., Le Toan, T., Mognard, N., Delbart, N., L'hermitte, J., & Vicente-Serrano, S. (2005). The impact of snow depth and snowmelt on the vegetation variability over central Siberia. *Geophysical Research Letters*, 32(21), L21412. <https://doi.org/10.1029/2005gl024286>
- Hanna, E., Fettweis, X., & Hall, R. (2018). Brief communication: Recent changes in summer Greenland blocking captured by none of the CMIP5 models. *The Cryosphere*, 12(10), 3287–3292. <https://doi.org/10.5194/tc-12-3287-2018>
- Hausfather, Z., & Peters, G. P. (2020). Emissions—the “business as usual” story is misleading. *Nature*, 577(7792), 618–620. <https://doi.org/10.1038/d41586-020-00177-3>
- Hersbach, H., Bell, B., Berrisford, P., Hirahara, S., Horányi, A., Muñoz-Sabater, J., et al. (2020). The ERA5 global reanalysis. *Quarterly Journal of the Royal Meteorological Society*, 146(730), 1999–2049. <https://doi.org/10.1002/qj.3803>
- Hirsch, A. L., Ridder, N. N., Perkins-Kirkpatrick, S. E., & Ukkola, A. (2021). CMIP6 multi-model evaluation of present-day heatwave attributes. *Geophysical Research Letters*, 48(22), e2021GL095161. <https://doi.org/10.1029/2021gl095161>
- Horton, R. M., Mankin, J. S., Lesk, C., Coffel, E., & Raymond, C. (2016). A review of recent advances in research on extreme heat events. *Current Climate Change Reports*, 2(4), 242–259. <https://doi.org/10.1007/s40641-016-0042-x>
- Hugelius, G., Loisel, J., Chadburn, S., Jackson, R. B., Jones, M., MacDonald, G., et al. (2020). Large stocks of peatland carbon and nitrogen are vulnerable to permafrost thaw. *Proceedings of the National Academy of Sciences of the United States of America*, 117(34), 20438–20446. <https://doi.org/10.1073/pnas.1916387117>
- Keuper, F., Wild, B., Kumm, M., Beer, C., Blume-Werry, G., Fontaine, S., et al. (2020). Carbon loss from northern circumpolar permafrost soils amplified by rhizosphere priming. *Nature Geoscience*, 13(8), 560–565. <https://doi.org/10.1038/s41561-020-0607-0>
- Konings, A., Williams, A., & Gentine, P. (2017). Sensitivity of grassland productivity to aridity controlled by stomatal and xylem regulation. *Nature Geoscience*, 10(4), 284–288. <https://doi.org/10.1038/ngeo2903>
- Kornhuber, K., & Tamarin-Brodsky, T. (2020). Future changes in northern hemisphere summer weather persistence linked to projected arctic warming. *Geophysical Research Letters*, 48, e2020GL091603. <https://doi.org/10.1029/2020gl091603>
- Lange, S., Volkholz, J., Geiger, T., Zhao, F., Vega, I., Veldkamp, T., et al. (2020). Projecting exposure to extreme climate impact events across six event categories and three spatial scales. *Earth's Future*, 11(12), e2020EF001616. <https://doi.org/10.1029/2020ef001616>
- Larson, E. J., Schiferl, L. D., Commane, R., Munger, J. W., Trugman, A. T., Ise, T., et al. (2021). The changing carbon balance of tundra ecosystems: Results from a vertically-resolved peatland biosphere model. *Environmental Research Letters*, 17(1), 014019. <https://doi.org/10.1088/1748-9326/ac4070>
- Lenton, T. M., Held, H., Kriegler, E., Hall, J. W., Lucht, W., Rahmstorf, S., & Schellnhuber, H. J. (2008). Tipping elements in the Earth's climate system. *Proceedings of the National Academy of Sciences of the United States of America*, 105(6), 1786–1793. <https://doi.org/10.1073/pnas.0705414105>
- Liu, L., Gudmundsson, L., Hauser, M., Qin, D., Li, S., & Seneviratne, S. I. (2020). Soil moisture dominates dryness stress on ecosystem production globally. *Nature Communications*, 11(1), 1–9. <https://doi.org/10.1038/s41467-020-18631-1>
- Lorenz, R., Argüeso, D., Donat, M. G., Pitman, A. J., van den Hurk, B., Berg, A., et al. (2016). Influence of land-atmosphere feedbacks on temperature and precipitation extremes in the GLACE-CMIP5 ensemble. *Journal of Geophysical Research: Atmospheres*, 121(2), 607–623. <https://doi.org/10.1002/2015jd024053>
- Mann, M. E., Rahmstorf, S., Kornhuber, K., Steinman, B. A., Miller, S. K., Petri, S., & Coumou, D. (2018). Projected changes in persistent extreme summer weather events: The role of quasi-resonant amplification. *Science Advances*, 4(10), eaat3272. <https://doi.org/10.1126/sciadv.aat3272>
- McCarty, J. L., Smith, T. E., & Turetsky, M. R. (2020). Arctic fires re-emerging. *Nature Geoscience*, 13(10), 658–660. <https://doi.org/10.1038/s41561-020-00645-5>
- Miralles, D. G., Teuling, A. J., Van Heerwaarden, C. C., & De Arellano, J. V.-G. (2014). Mega-heatwave temperatures due to combined soil desiccation and atmospheric heat accumulation. *Nature Geoscience*, 7(5), 345–349. <https://doi.org/10.1038/ngeo2141>
- Nabizadeh, E., Hassanzadeh, P., Yang, D., & Barnes, E. A. (2019). Size of the atmospheric blocking events: Scaling law and response to climate change. *Geophysical Research Letters*, 46(22), 13488–13499. <https://doi.org/10.1029/2019gl084863>
- Oertel, C., Matschullat, J., Zurba, K., Zimmermann, F., & Erasmí, S. (2016). Greenhouse gas emissions from soils—A review. *Geochemistry*, 76(3), 327–352. <https://doi.org/10.1016/j.chemer.2016.04.002>
- Oh, Y., Zhuang, Q., Liu, L., Welp, L. R., Lau, M. C., Onstott, T. C., et al. (2020). Reduced net methane emissions due to microbial methane oxidation in a warmer arctic. *Nature Climate Change*, 10(4), 317–321. <https://doi.org/10.1038/s41558-020-0734-z>
- Overland, J. E., & Wang, M. (2021). The 2020 Siberian heat wave. *International Journal of Climatology*, 41(S1), E2341–E2346. <https://doi.org/10.1002/joc.6850>
- Perkins-Kirkpatrick, S., & Gibson, P. (2017). Changes in regional heatwave characteristics as a function of increasing global temperature. *Scientific Reports*, 7(1), 1–12. <https://doi.org/10.1038/s41598-017-12520-2>

- Pulliaainen, J., Aurela, M., Laurila, T., Aalto, T., Takala, M., Salminen, M., et al. (2017). Early snowmelt significantly enhances boreal springtime carbon uptake. *Proceedings of the National Academy of Sciences*, *114*(42), 11081–11086. <https://doi.org/10.1073/pnas.1707889114>
- Pulliaainen, J., Luojus, K., Derksen, C., Mudryk, L., Lemmetyinen, J., Salminen, M., et al. (2020). Patterns and trends of northern hemisphere snow mass from 1980 to 2018. *Nature*, *581*(7808), 294–298. <https://doi.org/10.1038/s41586-020-2258-0>
- Rahmstorf, S., & Coumou, D. (2011). Increase of extreme events in a warming world. *Proceedings of the National Academy of Sciences*, *108*(44), 17905–17909. <https://doi.org/10.1073/pnas.1101766108>
- Schär, C., Vidale, P. L., Lüthi, D., Frei, C., Häberli, C., Liniger, M. A., & Appenzeller, C. (2004). The role of increasing temperature variability in European summer heatwaves. *Nature*, *427*(6972), 332–336. <https://doi.org/10.1038/nature02300>
- Schewe, J., Gosling, S. N., Reyser, C., Zhao, F., Ciais, P., Elliott, J., et al. (2019). State-of-the-art global models underestimate impacts from climate extremes. *Nature Communications*, *10*(1), 1–14. <https://doi.org/10.1038/s41467-019-08745-6>
- Schumacher, D. L., Keune, J., Van Heerwaarden, C. C., de Arellano, J. V.-G., Teuling, A. J., & Miralles, D. G. (2019). Amplification of mega-heatwaves through heat torrents fuelled by upwind drought. *Nature Geoscience*, *12*(9), 712–717. <https://doi.org/10.1038/s41561-019-0431-6>
- Seabold, S., & Perktold, J. (2010). Statsmodels: Econometric and statistical modeling with python. In *9th python in science conference*.
- Selsted, M. B., van der Linden, L., Ibrom, A., Michelsen, A., Larsen, K. S., Pedersen, J. K., et al. (2012). Soil respiration is stimulated by elevated CO₂ and reduced by summer drought: Three years of measurements in a multifactor ecosystem manipulation experiment in a temperate heathland (climaite). *Global Change Biology*, *18*(4), 1216–1230. <https://doi.org/10.1111/j.1365-2486.2011.02634.x>
- Serreze, M. C., & Barry, R. G. (2011). Processes and impacts of Arctic amplification: A research synthesis. *Global and Planetary Change*, *77*(1–2), 85–96. <https://doi.org/10.1016/j.gloplacha.2011.03.004>
- Sherstyukov, B. G., & Sherstyukov, A. B. (2014). Assessment of increase in forest fire risk in Russia till the late 21st century based on scenario experiments with fifth-generation climate models. *Russian Meteorology and Hydrology*, *39*(5), 292–301. <https://doi.org/10.3103/s1068373914050021>
- Stéfanon, M., Drobinski, P., D'Andrea, F., Lebeaupin-Brossier, C., & Bastin, S. (2014). Soil moisture-temperature feedbacks at meso-scale during summer heat waves over Western Europe. *Climate Dynamics*, *42*(5), 1309–1324. <https://doi.org/10.1007/s00382-013-1794-9>
- Stott, P. A., Stone, D. A., & Allen, M. R. (2004). Human contribution to the European heatwave of 2003. *Nature*, *432*(7017), 610–614. <https://doi.org/10.1038/nature03089>
- Turetsky, M. R., Abbott, B. W., Jones, M. C., Anthony, K. W., Olefeldt, D., Schuur, E. A., et al. (2020). Carbon release through abrupt permafrost thaw. *Nature Geoscience*, *13*(2), 138–143. <https://doi.org/10.1038/s41561-019-0526-0>
- Van Oldenborgh, G. J., Philip, S., Kew, S., Vautard, R., Boucher, O., Otto, F., et al. (2019). *Human contribution to the record-breaking June 2019 heat wave in France* (p. 32). World Weather Attribution (WWA).
- Vermote, E. (2019). NOAA climate data record (CDR) of AVHRR leaf area index (LAI) and fraction of absorbed photosynthetically active radiation (FAPAR). Version 5. <https://doi.org/10.7289/V5TT4P69>
- Watts, J. D., Natali, S. M., Minions, C., Risk, D., Arndt, K., Zona, D., et al. (2021). Soil respiration strongly offsets carbon uptake in Alaska and northwest Canada. *Environmental Research Letters*, *16*(8), 084051. <https://doi.org/10.1088/1748-9326/ac1222>
- Witze, A. (2020). The Arctic is burning like never before—and that's bad news for climate change. *Nature*, *585*(7825), 336–337. <https://doi.org/10.1038/d41586-020-02568-y>
- Wu, R., & Chen, S. (2020). What leads to persisting surface air temperature anomalies from winter to following spring over mid-to high-latitude Eurasia? *Journal of Climate*, *33*(14), 5861–5883. <https://doi.org/10.1175/jcli-d-19-0819.1>
- Zhang, P., Jeong, J.-H., Yoon, J.-H., Kim, H., Wang, S.-Y. S., Linderholm, H. W., et al. (2020). Abrupt shift to hotter and drier climate over inner East Asia beyond the tipping point. *Science*, *370*(6520), 1095–1099. <https://doi.org/10.1126/science.abb3368>
- Zhang, X., Manzanedo, R. D., D'Orangeville, L., Rademacher, T. T., Li, J., Bai, X., et al. (2019). Snowmelt and early to mid-growing season water availability augment tree growth during rapid warming in southern Asian boreal forests. *Global Change Biology*, *25*(10), 3462–3471. <https://doi.org/10.1111/gcb.14749>
- Zhang, Y., Parazoo, N. C., Williams, A. P., Zhou, S., & Gentine, P. (2020). Large and projected strengthening moisture limitation on end-of-season photosynthesis. *Proceedings of the National Academy of Sciences of the United States of America*, *117*(17), 9216–9222. <https://doi.org/10.1073/pnas.1914436117>
- Zhou, S., Williams, A. P., Berg, A. M., Cook, B. I., Zhang, Y., Hagemann, S., et al. (2019). Land–atmosphere feedbacks exacerbate concurrent soil drought and atmospheric aridity. *Proceedings of the National Academy of Sciences of the United States of America*, *116*(38), 18848–18853. <https://doi.org/10.1073/pnas.1904955116>
- Zhou, S., Zhang, Y., Williams, A. P., & Gentine, P. (2019). Projected increases in intensity, frequency, and terrestrial carbon costs of compound drought and aridity events. *Science Advances*, *5*(1), eaau5740. <https://doi.org/10.1126/sciadv.aau5740>
- Zona, D., Gioli, B., Commane, R., Lindaas, J., Wofsy, S. C., Miller, C. E., et al. (2016). Cold season emissions dominate the arctic tundra methane budget. *Proceedings of the National Academy of Sciences of the United States of America*, *113*(1), 40–45. <https://doi.org/10.1073/pnas.1516017113>
- Zscheischler, J., Mahecha, M. D., Von Buttlar, J., Harmeling, S., Jung, M., Rammig, A., et al. (2014). A few extreme events dominate global inter-annual variability in gross primary production. *Environmental Research Letters*, *9*(3), 035001. <https://doi.org/10.1088/1748-9326/9/3/035001>